

# Development of Digital X-ray Image Sensor Using a Two-Dimensional Multiwire Proportional Chamber

Dong-Myung Lee\*, Jung-Byung Park, Do-Sung Kim<sup>1</sup> and Hee-Dong Kang

Department of Physics, Kyungpook National University, Taegu 702-701, Korea

<sup>1</sup>Department of Physics Education, Taegu University, Kyungsan 712-714, Korea

(Received June 26, 1995; accepted June 3, 1996)

**Key words:** MWPC, radiation image sensor, X-ray digital image, delay line, spatial frequency, position resolution, gray level

A multiwire proportional chamber (MWPC) radiation sensor for use in X-ray digital imaging systems is presented. The system consists of a 2-D MWPC radiation image sensor filled with Ar gas and standard NIM/CAMAC radiation position readout electronics. The X-ray image performance of the system is demonstrated using a test mask made of a copper sheet with letter-shaped holes cut out of it. Reconstructed images of the X-ray projection through several objects are also presented. The digital X-ray image system has submillimeter position resolution and the advantages of easy data manipulation and display of digitally stored data.

## 1. Introduction

Since ionizing radiation emitted in nuclear or atomic processes cannot be detected by humans, it is detected by transducers capable of absorbing radiation energy and subsequently converting it into electrical signals. In the multiwire proportional chamber (MWPC), the electrical signals come from the charge produced by the ionization of gas by incident radiation and the electron avalanche produced by the applied electric field. Currently the MWPC is used as a basic X-ray image transducer or radiation visual sensor

---

\*Present address: Environment Assessment Department, Korea Institute of Nuclear Safety, P. O. Box 114, Yuseong, Taejeon, Korea

in material science,<sup>(1,2)</sup> medicine,<sup>(3,4)</sup> molecular biology<sup>(5,6)</sup> and astronomy.<sup>(7)</sup>

Recently, improvements and advances in personal computer technology including high-powered, low-cost microprocessors, large memories, fixed storage devices and sophisticated high-resolution color displays at reasonable cost have made it possible to use digital image processing for a wide range of applications. Digital image processing coupled with an X-ray image sensor based on a MWPC can be used in new experimental devices which require high precision, high-time-resolution measurements.

Especially in diagnostic radiology,<sup>(8)</sup> digital X-ray imaging systems based on a 2-D MWPC have several advantage, namely, (i) reducing the irradiation dose, (ii) improving diagnostic accuracy and (iii) using a flexible real-time display without complex, time-consuming intermediate steps which were previously unavoidable. An additional advantage is the storage capability of image data which can be immediately sent and received through a computer network.

MWPCs also have many advantages,<sup>(9)</sup> which are not readily obtainable using other radiation image sensors, such as high efficiency, good spatial resolution, good position linearity, good timing resolution, high counting rate capability and a large variety of sensing areas. To make use of these advantages, we have been developing 2-D MWPC soft X-ray image sensors for the last three years. The operating and position sensing characteristics of one- or two-dimensional MWPCs have already been reported.<sup>(10,11)</sup>

We report the imaging capabilities of a 2-D MWPC coupled with an electronic readout system, which consists of fast NIM standard modules and CAMAC software compatible with IBM PC/AT. Several X-ray images of test objects are also shown.

## 2. 2-D MWPC X-ray Image Sensor

The 2-D MWPC X-ray image sensor was developed for use in experiments involving a synchrotron radiation source as the X-ray image transducer using an artificial delay line readout method. The primary design and construction are based on gas counter principles in which positions are characterized by the charge distributions induced on cathode planes by an avalanche surrounding an anode wire.

A gas-flow 2-D MWPC was used with an effective sensing area of 100 mm × 100 mm and a photon conversion depth of 6.5 mm. Fine anode wires of gold-plated tungsten, 20 μm in diameter, were spaced at 2 mm intervals in a plane, and two cathode planes were located above and below at distances of 3 mm and 3.5 mm from the anode plane, respectively. The upper cathode plane consisted of 50 μm gold-plated tungsten wires at 2 mm intervals and the lower cathode plane consisted of gold-plated copper strips 1.6 mm wide on printed circuit boards at the same interval. The upper cathode wires and lower cathode strips were perpendicular to each other, and the upper cathode wires were parallel to the anode wires. The artificial delay lines used to delay the signals from the cathode wires and strips were fabricated on a printed circuit board using passive capacitor and inductor components with accuracies of about ±1% from the nominal values.

The gas chamber is made of a cylindrical stainless steel containment vessel which has an X-ray entrance window on the upper flange and electrical connections on the lower

flange. The containment vessel and the flanges are sealed with O-rings. Two windows are installed, namely, an inner window consisting of 25- $\mu\text{m}$ -thick aluminized Mylar film which serves as an electrical ground plane and an outer window made of 100- $\mu\text{m}$ -thick polypropylene film which serves as a gas-tight frame. The position sensing components are mounted in the gas chamber. The 2-D MWPC is operated with a gas mixture of 90% argon and 10% methane, or 90% argon and 10% carbon dioxide at 1 atm. Figure 1 shows the position sensing components which consist of the anode wires, lower cathode strips and upper cathode wires with delay lines.<sup>(1)</sup>

### 3. Image Readout Electronic System

The position information from MWPCs is obtained in terms of a weighted centroid of charge collected or induced on the electrodes. The centroid is usually determined by a delay line or charge division method. Alternatively, it can be determined by computing the outputs from discrete wires. We have chosen the delay line method, since it is relatively simple and inexpensive.

The avalanche created by an incident X-ray induces pulses on an anode wire and on two orthogonal cathodes, resulting in an anode signal and four cathode signals from the ends of the two cathodes. The coordinates of an X-ray interaction point are determined from the arrival time difference between the signals at the ends of the delay lines. The X-ray image

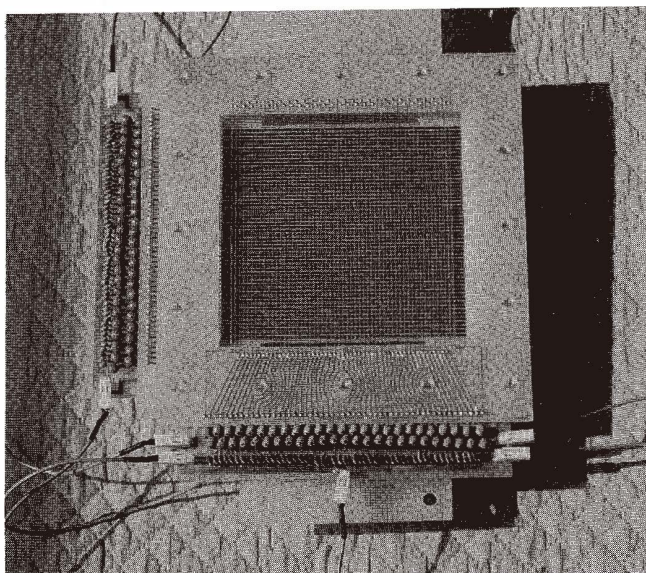


Fig. 1. A photograph of the X-ray image sensing components.

readout electronic system is shown in Fig. 2.

The readout system consists of three types of components; five preamplifiers, five constant fraction discriminators (CFDs) and a time-to-digital converter (TDC). The preamplifiers terminate and amplify the signals from the ends of the delay lines, the CFDs produce accurate timing pulses using the outputs of the preamplifiers and the TDC converts the time between the anode pulse and the cathode pulse from the end of a delay line into a number proportional to the coordinate of the interaction point in the 2-D MWPC.

The cathode signals from the MWPC are sent to four preamplifiers with a delay of 1  $\mu\text{s}$ , and the anode signal from the MWPC is sent to a preamplifier with no delay. The delayed

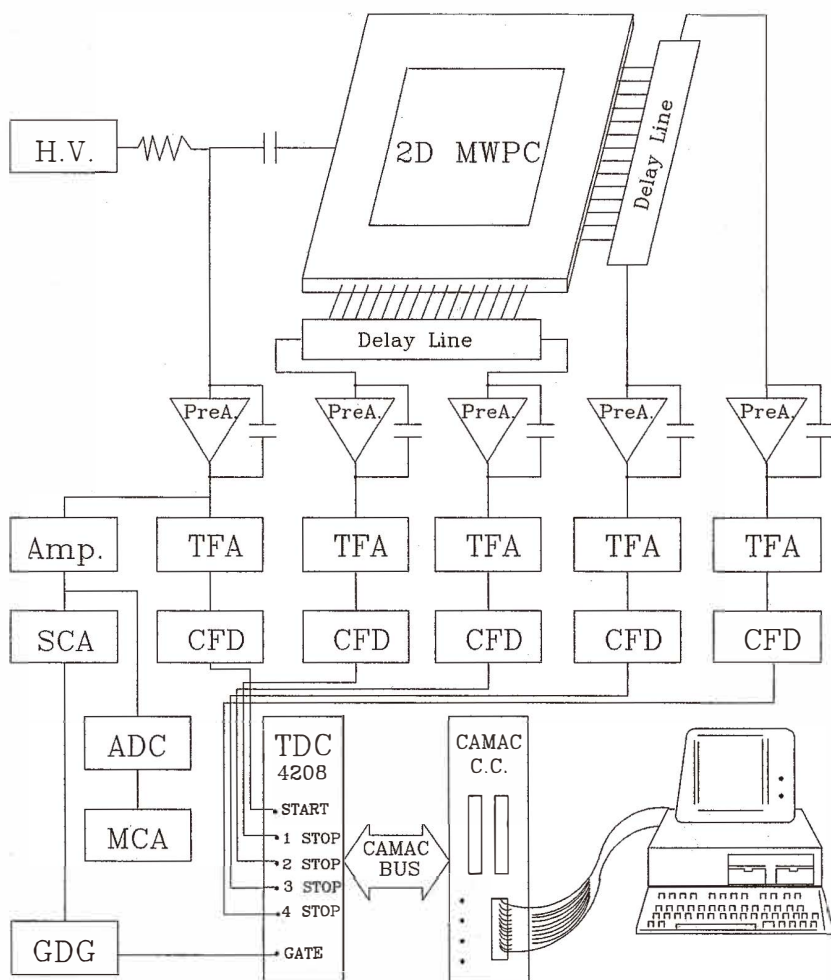


Fig. 2. Block diagram of the 2-D MWPC X-ray image readout electronic system.

signals are actively terminated and separately amplified by four charge-sensitive preamplifiers using feedback capacitors of 2 pF and resistors of 100 M $\Omega$ .<sup>(12)</sup>

The anode and four cathode signals are further shaped and amplified using a timing filter amplifier (TFA, CANBERRA 2111). The outputs from the TFA are discriminated using a CFD (CANBERRA 2126Q). The anode output pulse is used as the gate for a CAMAC multihit TDC (LeCroy 4208) via a single channel analyzer (SCA, ORTEC 550) which discriminates and filters out unreasonable signals such as electronic noise or leakage current due to the applied voltage at the anode. If the anode pulse height criterion for Cu  $K\alpha$  X-rays is satisfied at the SCA, the event is considered to be valid. Simultaneously, the anode output pulse is sent to a common START in TDC. The cathode signals from the CFDs are transferred to STOP in the 8-channel TDC.

The multihit TDC measures the time between the leading edge of the common START pulse (anode signal) and the leading edge of the corresponding STOP pulse (four cathode signals). Figure 3 shows the logic timing waveforms from the independent STOP channels. If one or more of the four cathode signals are missing, the event is considered to be invalid and the data are discarded.

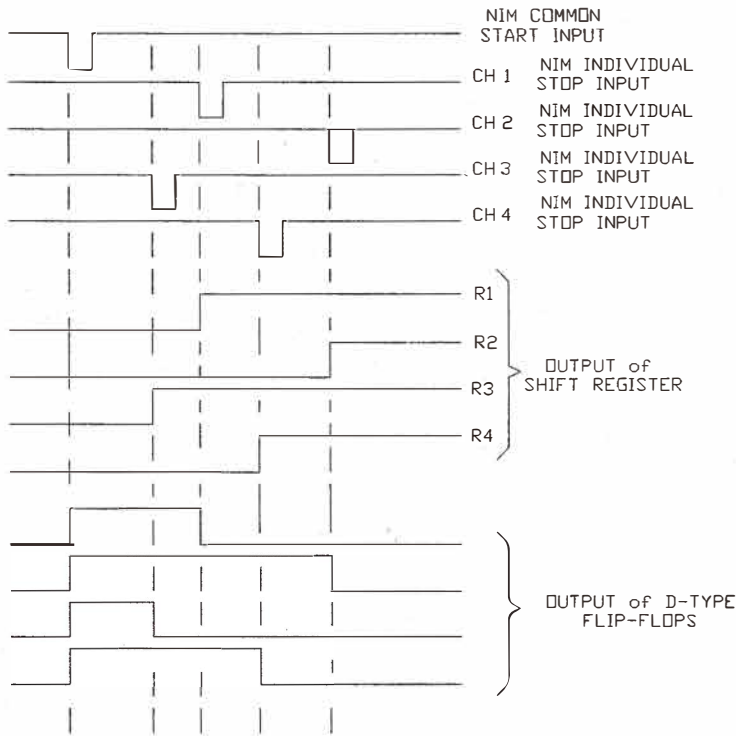


Fig. 3. Logic timing waveforms from four independent channels.

#### 4. Digital X-ray Image Processing

The CAMAC system is connected to an IBM PC/AT with a commercially available controller/interface (6002 and PC004, DSP technology, Inc.). The data in the multihit TDC are transferred to the computer via a CAMAC bus for each CAMAC cycle.

A control program allows convenient access to both programmed I/O and DMA facilities of the PC004/6002 combination via a variety of interpretive and compiled high-level programming languages for personal computers. The readout data are directly transferred into the computer memory in  $100 \times 100$  8-bit words and permanently stored on a hard or floppy disk.

Using the data stored in the computer memory, an image processing program in C language displays in real time an X-ray projection image which consists of a matrix of  $100 \times 100$  pixels with 256 colors or gray levels. The X-ray images are displayed on a color monitor via a video graphics array (VGA) driver.

Figures 4 and 5 show a flow chart of the image processing program, and a photograph of the X-ray imaging system and the test X-ray tube, respectively.

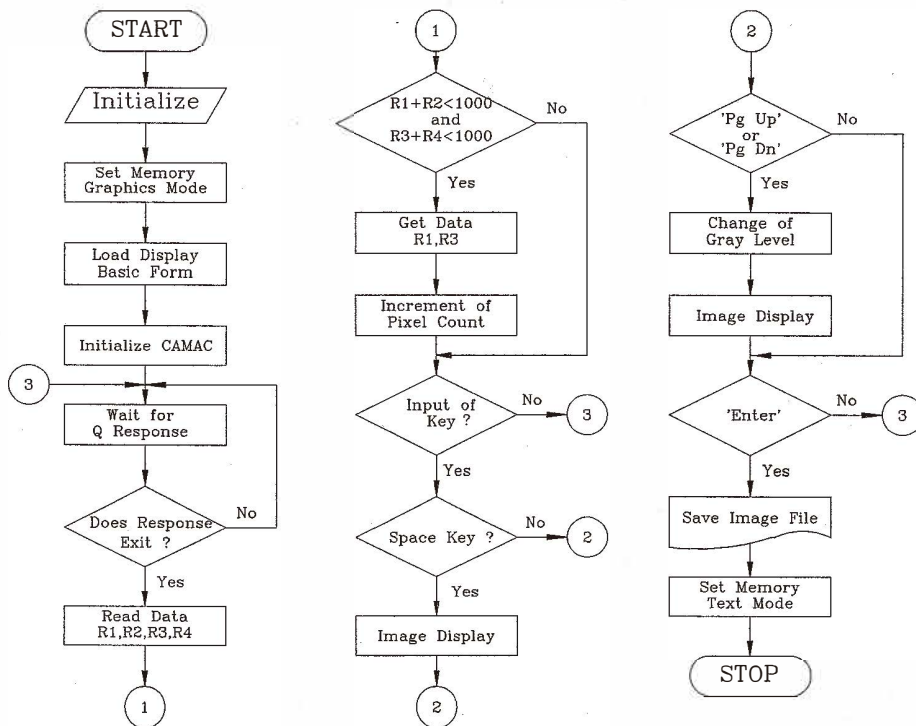


Fig. 4. Flow chart of the X-ray image processing program.

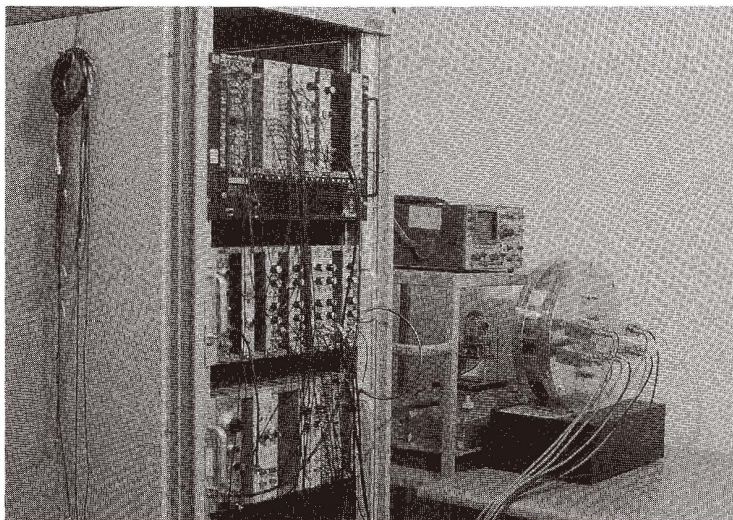


Fig. 5. A photograph of the X-ray imaging system and the test X-ray tube.

## 5. Experimental Results

The imaging performance of the 2-D MWPC was tested using Cu  $K\alpha$  X-rays (8.04 keV). The 2-D MWPC was filled with a gas mixture of Ar (90%) and  $\text{CH}_4$  (10%) at room temperature and pressure. Some of the characteristics of the 2-D MWPC have already been reported in previous papers.<sup>(11,12)</sup> In this study, we examined the X-ray image quality using the X-ray patterns obtained from the test mask and several objects.

Figure 6(a) shows the X-ray image obtained in the direction parallel to the anode wires for 8.04 keV X-rays passing through an Al test mask, which has three holes 0.2 mm in diameter at 2 mm intervals. Figure 6(b) shows the measured X-ray position spectrum for the Al mask. We studied the position resolution (FWHM) at 2 mm intervals in the direction parallel to the anode wires. The measured position resolution in Fig. 6(b) was about 0.70 mm (FWHM). We measured the electronic noise contribution to the position resolution by sending a signal from a pulse generator through the readout system. The electronic noise contribution to the position resolution was about 0.15 mm (FWHM) as shown on the left and right sides of Fig. 6(b).

For many practical purposes, it is more convenient to describe the spatial resolution in terms of the contrast versus spatial frequency response function (CFR), namely, the spatial frequency at a defined level of contrast. In order to measure the spatial frequency, we used a set of opaque grids for X-rays with widths of 1 mm, 1.5 mm and 2 mm which produce periodic images. The results of these measurements are shown in Fig. 7. The contrast is 0.28 at the spatial frequency (1/mm) of 0.23 in the case of a maximum of 1024 events per unit pixel.

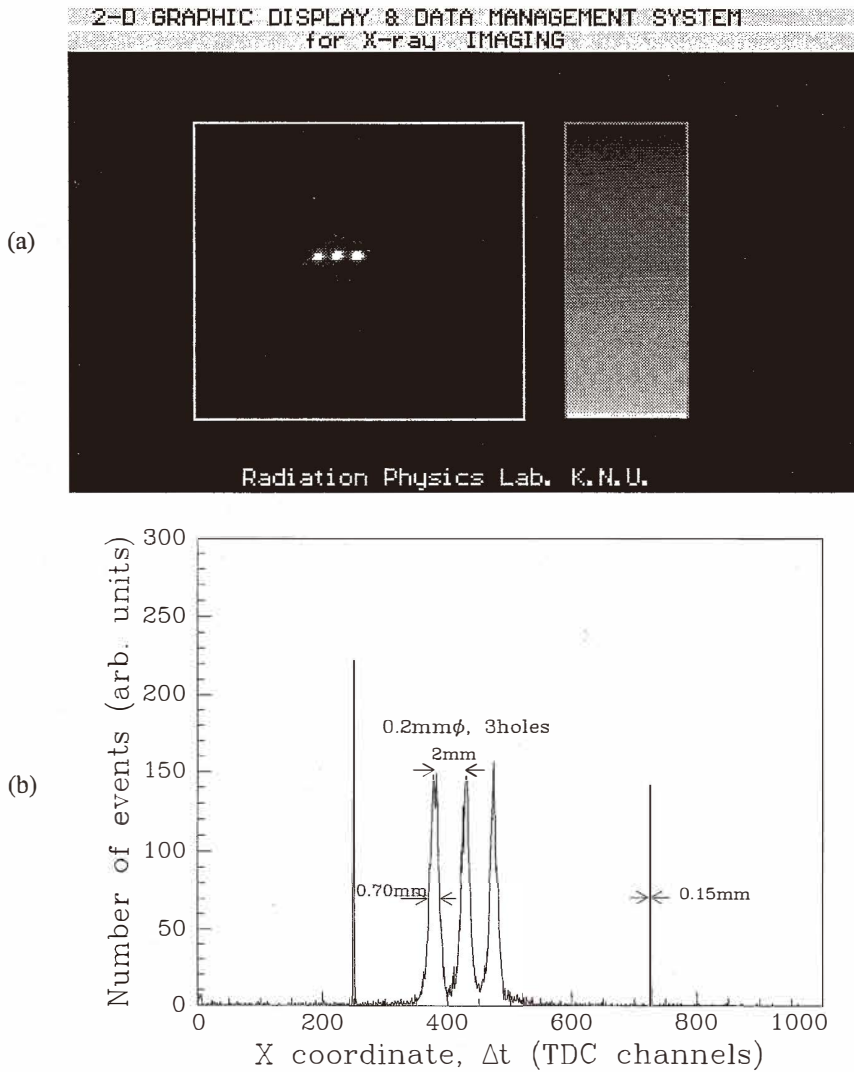


Fig. 6. Position resolution for X-ray beam passing through three holes, in the direction parallel to the anode wires; (a) X-ray image of holes, (b) distribution of time difference.

Figure 8 shows the image brightness as a function of the transmitted X-ray flux through a polypropylene film wedge. In this figure, the brightness of 100 events per unit pixel corresponds to that of direct X-ray flux. The linearity deteriorates in the low X-ray flux region, but improves as the X-ray flux increases.

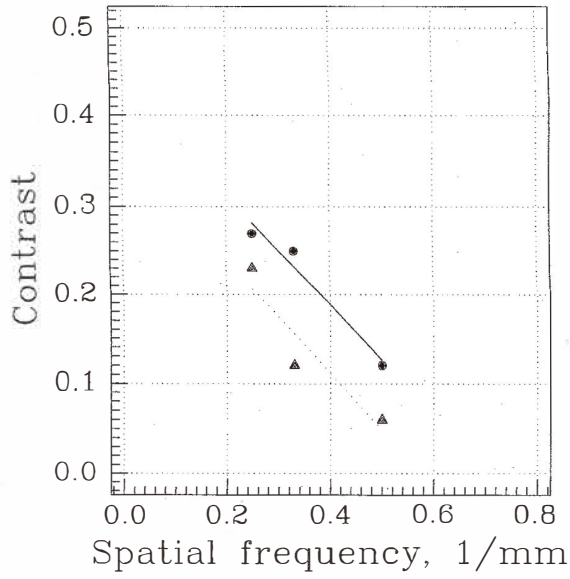


Fig. 7. Contrast versus spatial frequency.

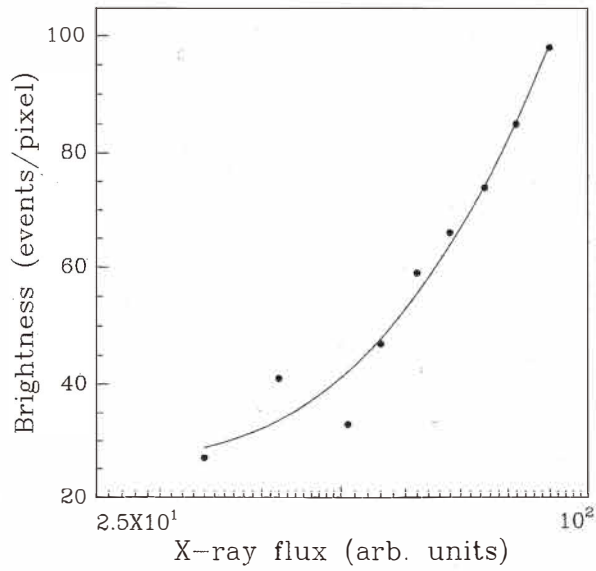


Fig. 8. Image brightness as a function of the transmitted X-ray flux.

Figure 9 shows an image of a saw-toothed gear on the computer terminal screen. The image quality depends not only on the spatial resolution but also on the maximum gray levels. In Fig. 9, the two images have the same spatial resolution, but different maximum gray levels. In Fig. 9(a), each pixel may take a value between 0 and 255, with 0 indicating black and 255 indicating white. In Fig. 9(b) the number of values for each pixel is only 8, 0 to 7. Even though the spatial resolution (pixels/sensor length) remains the same, the image becomes coarser due to the reduced gray level.

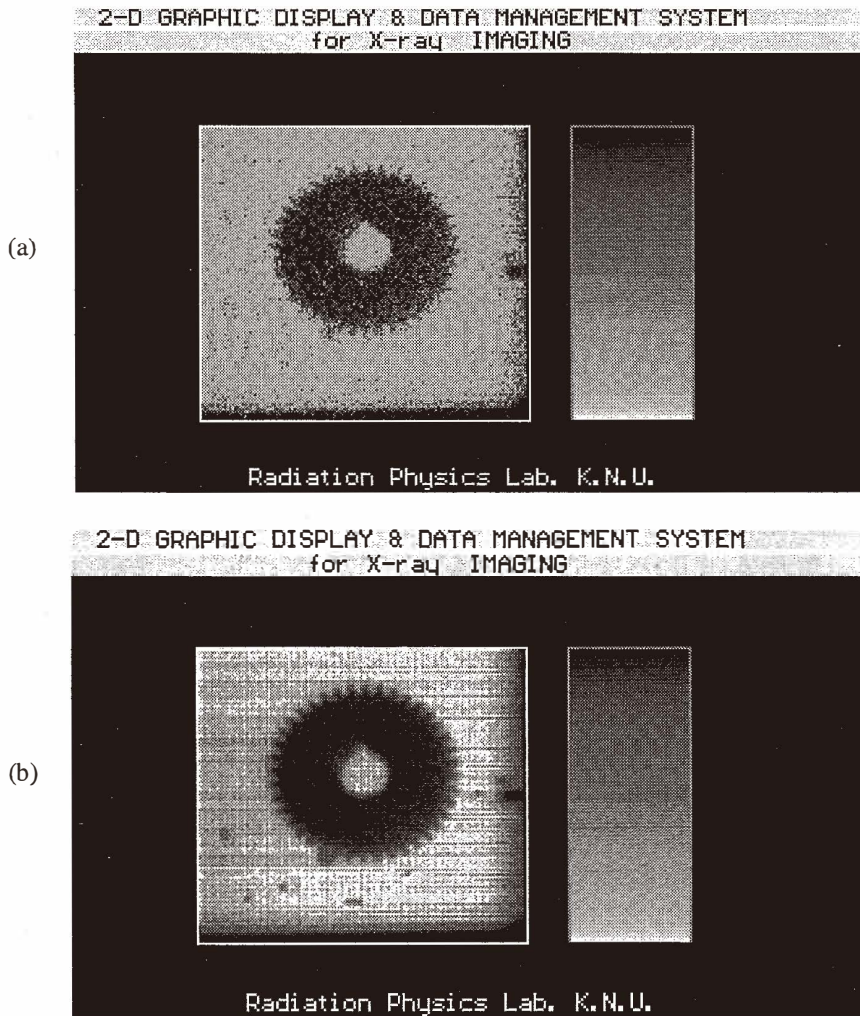


Fig. 9. Reconstructed image of a saw-toothed gear: (a) 8 gray levels, (b) 256 gray levels.

Figure 10(a) shows a photograph of a test mask made of a copper sheet with letter-shaped holes cut out of it. The actual size of the letters is 72-point font (height 18 mm, width 4 mm). Figure 10(b) shows the image on the computer terminal screen obtained by irradiating X-rays for one minute on the test mask, which was placed in front of the X-ray window of the 2-D MWPC.

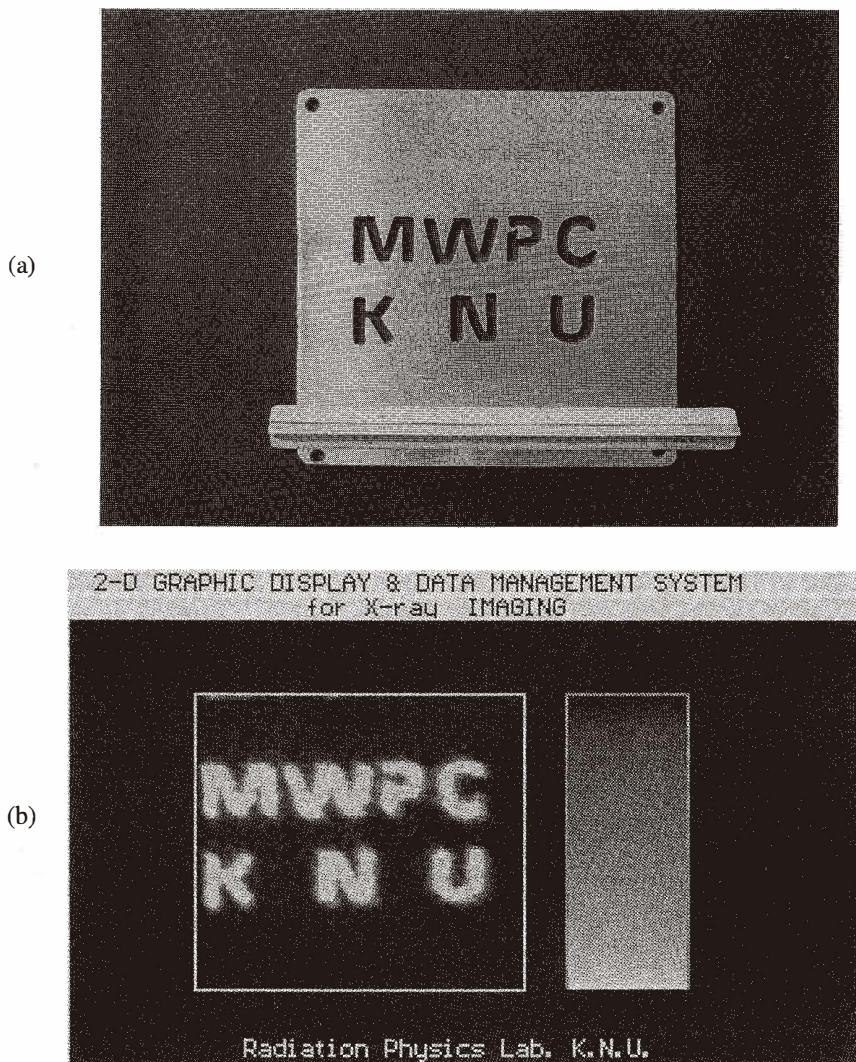


Fig. 10. (a) A photograph of the test mask made of copper sheet and (b) the X-ray image reconstructed by the 2-D MWPC.

## 6. Conclusions

The digital imaging system described in this paper is potentially useful for X-ray imaging applications. The system has submillimeter spatial resolution and the digital nature of the reconstructed images allows the acquisition of quantitative information and the storage of image files for easy manipulation or real-time display.

At present, the system is limited by the counting rate performance. In the future, we plan to upgrade the counting rate capability by using a fast histogramming buffer memory and different delay time, wire spacing and position readout method.

## Acknowledgments

This work was supported in part by the Pohang Accelerator Laboratory Research Fund (Contract No. 94-001D) and in part by the Sensor Technology Research Center, Kyungpook National University. We would like to thank Professors K. B. Lee and T. N. Lee of the Dept. of Physics, POSTECH, for their kind support.

## References

- 1 R. Lewis, J. S. Worgan, N. S. Fore, F. d'Annunzio, C. Hall and B. Parker: Nucl. Instru. Meth. **A310** (1991) 70.
- 2 R. A. Lewis, N. S. Fore, W. Helsby, C. Hall, A. Tones, B. Parker, I. Summer, J. S. Worgan and C. Budtz-Jorgensen: Rev. Sci. Instru. **63**(1) (1992) 642.
- 3 E. A. Babichev, S. E. Baru, A. G. Khabakhpashev, G. M. Kolachev, O. A. Ponomarev, G. A. Savinov and L. I. Shekhtman: Nucl. Instru. Meth. **A323** (1992) 49.
- 4 R. Bellazzini, A. Brez, A. Del Guerra, M. M. Massai, M. R. Torquati, M. Franchini and G. Perri: Nucl. Instru. Meth. **228** (1984) 193.
- 5 J. E. Bateman, J. F. Connelly, R. Stephenson, A. C. Flesher, C. J. Bryant, A. D. Lincoln, P. A. Tucker and S. W. Swanton: Nucl. Instru. Meth. **A259** (1987) 506.
- 6 K. Hesagawa, K. Mochiki, M. Koike, Y. Satow, H. Hashizume and Y. Itaka: Nucl. Instru. Meth. **A252** (1986) 158.
- 7 P. B. Reid, W. H. M. Ku, K. S. Long, R. Novick and R. L. Pisarski: IEEE Trans. Nucl. Sci. NS-**26** (1981) 47.
- 8 E. A. Babichev, S. E. Baru, A. G. Khabakhpashev, G. M. Kolachev, G. A. Savinov, L. I. Shekhtman, V. A. Sidorovo and A. I. Volobuev: Nucl. Instru. Meth. **A310** (1991) 449.
- 9 G. C. Smith: Nucl. Instru. Meth. **222** (1984) 230.
- 10 D. -M. Lee, H. -D. Choi and H. -D. Kang: New Phys. **34**(2) (1994) 154.
- 11 D. -M. Lee, H. -D. Choi and H. -D. Kang: Korean Appl. Phys. **7**(4) (1994) 326.
- 12 R. A. Boie, J. Fischer, Y. Inagaki, F. C. Merritt, V. Radeka, L. C. Rogers and D. M. Xi: Nucl. Instr. Meth. **201** (182) 93.